Available online at www.sciencedirect.com
ScienceDirect
International Journal of Heat and Fluid Flow 29 (2008) 35–47
International Journal of HEAT AND FLUID FLOW
www.elsevier.com/locate/ijhff

Modeling the flow in a 90° rectangular duct using one Reynolds-stress and two eddy-viscosity models

K. Yakinthos *, Z. Vlahostergios, A. Goulas

Laboratory of Fluid Mechanics and Turbomachinery, Department of Mechanical Engineering, Aristotle University of Thessaloniki, 54124 Thessaloniki, Greece

Received 10 October 2006; received in revised form 4 May 2007; accepted 14 May 2007
Available online 9 July 2007

Abstract

A new effort to model the flow in a 90° rectangular duct by adopting three low-Reynolds-number turbulence models, two eddy-viscosity models (a linear and a non-linear) and a Reynolds-stress model, is presented. The complex flow development is a challenge for the application of turbulence models in order to assess their capability to capture the secondary flow and the developing vortices due to curvature and strong pressure gradient effects. The numerical results show that both the non-linear eddy-viscosity and the Reynolds-stress models can provide good results, especially for the velocity distributions. The superiority of the Reynolds-stress model is shown primarily in the Reynolds-stress distributions, which have the best quality among the predictions from the other models. On the other hand, the main advantage of the non-linear model is its simplicity and the smaller needed CPU cost, compared to the Reynolds-stress model. Additionally, in some stations of the flow development, the non-linear model provides good velocity distributions. The linear model gives lower quality predictions for the Reynolds-stress distributions, although it is capable in providing quite satisfactory results for the velocity distributions.

Keywords: Curved duct; Non-linear eddy-viscosity model; Reynolds-stress model

1. Introduction

In many areas of mechanical engineering, there is a need to model the flow through simple geometries involving complex flow field development. A typical example is the flow through closed straight or curved ducts. These flow fields present large recirculation zones, secondary vortices and in general, three-dimensional phenomena. Usually, the flow field is developed as fully turbulent and in relation with the three-dimensional developing phenomena, the use of an accurate turbulence model is nearly obligatory. A characteristic example of such flow configurations is the flow field development in an automotive engine air-manifold or in the inlet duct of a turbo-compressor device. Another example can be found in the pump industry where a preliminary design is usually performed by modeling the passage through a centrifugal pump with a curved duct. A correct modeling of these flow fields can provide all the necessary information for the accurate design of these devices regarding in most cases the efficiency coefficient. On the other hand, there are situations where the experiments for these configurations are very difficult to be carried out and with a noticeable cost. Nowadays, the engineer has available powerful CFD commercial packages designed to use the most advanced numerical schemes and grid utilities. These tools are also supported by a plethora of turbulence models. Until now, the industry has focused on "quick and costless solutions", but since the upper limits of design have been pushed upwards, new needs are arising focusing on the very accurate predictions which have the potential to improve the operation of an engineering product. The research in the area of turbulence modeling is still in progress and various formulations of more

* Corresponding author.
E-mail address: kyak@auth.gr (K. Yakinthos).

0142-727X/$ - see front matter © 2007 Elsevier Inc. All rights reserved.
doi:10.1016/j.ijheatfluidflow.2007.05.006

Nomenclature

$c_1, c_2, c_3, c_4, c_5, c_\mu$	turbulence parameters (linear and non-linear eddy-viscosity models)
d_{ij}	diffusion term (Reynolds-stress model)
d_{ijk}	diffusion term in the triple moments correlation (Reynolds-stress model)
H	duct width
k	turbulent kinetic energy
P_{ij}	turbulence production term (Reynolds-stress model)
P^1_{ijk}	production term in the triple moments correlation (Reynolds-stress model)
P^2_{ijk}	production term in the triple moments correlation (Reynolds-stress model)
S_{ij}	mean strain-rate tensor
$\widetilde{S}$	dimensionless strain parameter
U_0	duct inlet velocity

Greek symbols

δ_{ij}	Kronecker delta
ε	dissipation rate of k
$\tilde{\varepsilon}$	"homogeneous" dissipation rate of k
ε_{ij}	dissipation (Reynolds-stress model)
ε_{ijk}	dissipation term in the triple moments correlation
ν	kinematic viscosity
ν_t	eddy-viscosity (linear and non-linear eddy-viscosity models)
Π_{ij}	pressure correlation (Reynolds-stress model)
ϕ_{ijk}	pressure correlation term in the triple moments correlation (Reynolds-stress model)
Ω_{ij}	mean vorticity tensor
$\widetilde{\Omega}$	dimensionless vorticity parameter

sophisticated models than the classical standard k–ε model are forthcoming. During the previous decade, the Reynolds-stress models (RSM) have taken a central position in the turbulence modeling field while, new alternative formulations such as explicit algebraic stress models or non-linear eddy-viscosity models (NLEVM) have been developed. The general sense is that the RSMs have the potential to provide more accurate results. The NLEVMs are a hybrid formulation between the linear eddy-viscosity models and RSMs, they are simpler to adopt in a Navier–Stokes solver and they have been tested in numerous flow configurations. The numerical results show that they can provide satisfactory solutions, better than the ones obtained by the linear models. In general, RSMs are very complicated, and they require a lot of programming effort and increased CPU power. Additionally, in some cases, they can present an unstable behavior during an iterative procedure, thus further numerical techniques are needed in order to obtain a stable and successful convergence.

Returning back to the complex flow configurations, the flow in a closed duct is primarily characterized by the existence of finite walls, which enclose the flow. A curved configuration of a closed duct generates high-pressure differences from the convex to the concave wall, leading to a flow governed by strong pressure and curvature effects. The importance of the phenomena developing through a curved duct has been shown many times in the past by numerous experiments in setups of ducts having various configurations such as different cross-sections (circular or rectangular), different inner and outer diameters, or even different bowing (U-ducts or 90° ducts), see for example the experiments of Ellis and Joubert (1974), Smits et al. (1979), Monson et al. (1990), Davis and Gessner (1992) and Cheah et al. (1994). In the present work, the 90° rectangular duct configuration has been chosen. The experimental data have been provided by the ERCOFTAC site and refer to the measurements of Kim and Patel (1993) using the pressure probe and hot-wire measurement techniques. They are very detailed and cover the majority of the cross-sections where major full 3D flow phenomena are developing. The main mechanism of the flow development is based on the formation of two symmetrical vortices in the cross-sectional direction in the curved region leading to strong secondary motions. The computed Reynolds number using the duct width $H = 0.203$ mm and the inlet velocity $U = 16$ m/s, is equal to 224,000. The advantage of the detailed measurements is that they can be used as a reference for the validation of turbulence models and, this is the reason for the large number of publications, where attempts of modeling these types of flows have been presented. A literature survey has shown that the UMIST group, has made a very significant contribution which has been proven very helpful for the derivation and evaluation of the new variants of turbulence models especially suitable for the modeling of rotating and heated ducts presented by the same group. Examples of this effort are the publications of Craft et al. (1996), Iacovides et al. (1996a,b). Tamamidis and Assanis (1993) have performed computations in a 90° curved duct of square cross-section but they were primarily focused on the accuracy of the numerical schemes adopted in order to obtain satisfactory velocity distributions with the use of an elliptic Navier–Stokes solver. For the case of a U-duct, Rumsey et al. (2000) presented results by adopting the Spalart–Almaras one equation model, the two-equation SST model and the Gatski and Speziale (1993) explicit algebraic stress model. They concluded that none of the three models could capture the flow parameters especially in the convex wall of the duct although a full RSM does (they did not include further detailed information for the adopted RSM). Sotiropoulos and Ventikos (1998) presented results for the same duct as the present one by adopting four two-equation

models, two LEVM (the two-layer k–ε and the k–ω model) and two NLEVM based on the k–ω formulations of Abid et al. (1995) and Sofialidis and Prinos (1996) using the quadratic model of Gatski and Speziale (1993) and the cubic model of Craft et al. (1996), respectively. They concluded that the isotropic linear models were "inaccurate for resolving complex three-dimensional flow" while the model of Craft et al. (1996) yielded the best overall predictions especially for the Reynolds stresses.

In the present work, the flow modeling was performed by using three different turbulence models, the Launder and Sharma (1974) low-*Re*-number k–ε model, the Craft et al. (1996) NLEVM and the RSM of Craft (1998) which is an alternative low-*Re*-number formulation of Craft and Launder (1996) model. The choice of these models has been made for the following reasons: the LEVM has been used widely in the industry (in the majority of the commercial CFD codes this model is included) and it is still a first choice for a quick and stable prediction of complex flow fields, despite its well-known deficiencies primarily related to its isotropic behavior. The CLS NLEVM has been used in a large variety of flow setups and it has been proven that it can provide very satisfactory predictions, even in transitional flows, Craft et al. (1997), Palikaras et al. (2002, 2003), it is quite stable during an iterative procedure (by adopting quite simple stabilizing measures) and it needs a small amount of programming effort. Additionally, Sotiropoulos and Ventikos (1998) concluded that this cubic formulation provided better predictions than the quadratic formulation of Gatski and Speziale (1993). The Reynolds-stress model of Craft (1998) is a relatively new model. Although it is a quite complex model, it has the advantage of not using any wall distance, an aspect that is found to be very difficult to implement when a three-dimensional flow with walls is considered.

The computational results for the velocity field and Reynolds stress distributions are presented in detailed comparisons with the available experimental data and a grid independency study is performed for three grids.

The modeling of this flow setup has been motivated by the desire to investigate the performance of advanced turbulence models presented so far. In most cases an engineer is asking questions regarding primarily their capability to provide good results combined with an ease of applicability. Additionally, the standard engineer's question is "is it worth proceeding with a model that in most cases is quite complex, difficult to program and time-consuming for a complicated flow configuration?" Through the following sections an attempt will be made to answer to these questions.

2. Brief description of the adopted models

2.1. The linear and non-linear eddy-viscosity model

The first model is the Launder and Sharma (1974) LEVM. Since it has been a widely used and referenced model, no details will be provided. The Craft et al. (1996) model is based on a cubic constitutional expression for the Reynolds-stresses:

$$\begin{aligned}\overline{u_i'u_j'} &= \frac{2}{3}k\delta_{ij} - \nu_t S_{ij} + c_1\frac{k}{\tilde{\varepsilon}}\nu_t\left(S_{ik}S_{kj} - \frac{1}{3}S_{kl}S_{kl}\delta_{ij}\right)\\ &+ c_2\frac{k}{\tilde{\varepsilon}}\nu_t(\Omega_{ik}S_{kj} + \Omega_{jk}S_{ki}t)\\ &+ c_3\frac{k}{\tilde{\varepsilon}}\nu_t\left(\Omega_{ik}\Omega_{kj} - \frac{1}{3}\Omega_{kl}\Omega_{kl}\delta_{ij}\right) + c_4\frac{k^2}{\tilde{\varepsilon}^2}\nu_t(S_{ki}\Omega_{lj}\\ &+ S_{kj}\Omega_{li})S_{kl} + c_5\frac{k^2}{\tilde{\varepsilon}^2}\nu_t(S_{kl}S_{kl} - \Omega_{kl}\Omega_{kl})S_{ij} \end{aligned} \quad (1)$$

where $S_{ij} = \left(\frac{\partial \overline{U}_i}{\partial x_j} + \frac{\partial \overline{U}_j}{\partial x_i}\right), \Omega_{ij} = \left(\frac{\partial \overline{U}_i}{\partial x_j} - \frac{\partial \overline{U}_j}{\partial x_i}\right)$ and $c_1 = -0.1$, $c_2 = 0.1, c_3 = 0.26, c_4 = -10c_\mu^2, c_5 = -5c_\mu^2$.

The model solves the set of turbulent kinetic energy and turbulent dissipation rate transport equations. Since it is a low-Reynolds number model it uses a damping function for the eddy viscosity. Additionally, for the calculation of the eddy viscosity, the c_μ coefficient is "strain-sensitized" and instead of having the typical constant value equal to 0.09 it is computed from an alternative expression using the dimensionless strain and vorticity parameters:

$$\widetilde{S} = \frac{k}{\tilde{\varepsilon}}\sqrt{1/2S_{ij}S_{ij}}, \quad \widetilde{\Omega} = \frac{k}{\tilde{\varepsilon}}\sqrt{1/2\Omega_{ij}\Omega_{ij}}$$

2.2. The low-Reynolds-number Reynolds-stress model

The low-Reynolds number RSM is a further development of the Craft and Launder (1996) Reynolds-stress model, which is based on the two-component-limit concept. Craft (1998), in order to enhance the accuracy of the two-component-limit behavior near the walls, introduced some extra terms into the pressure correlation. The model solves the following stress-transport equation:

$$\frac{\mathrm{D}\overline{u_iu_j}}{\mathrm{D}t} = P_{ij} + \Pi_{ij} - \varepsilon_{ij} + d_{ij} \quad (2)$$

where P_{ij} is the production of turbulence, Π_{ij} is the pressure correlation term, ε_{ij} is the dissipation rate and d_{ij} is the diffusion term. Only the term corresponding to the production of turbulence does not require any modeling. Details for these terms can be found in the paper of Craft (1998) but a discussion will be made regarding especially the diffusion term. This term is represented by the expression:

$$d_{ij} = \frac{\partial}{\partial x_k}\left(\nu\frac{\partial \overline{u_iu_j}}{\partial x_k} - \overline{u_iu_ju_k}\right) \quad (3)$$

and includes the term of the triple correlations (turbulent diffusion) which needs further modeling. Craft presented an alternative approach for the triple correlations, instead of adopting the expression of Hanjalic and Launder (1972). He used the transport equation for the triple correlations:

$$\frac{\mathrm{D}\overline{u_iu_ju_k}}{\mathrm{D}t} = P_{ijk}^1 + P_{ijk}^2 + \phi_{ijk} + d_{ijk} - \varepsilon_{ijk} \quad (4)$$

The first two terms, appearing in the right hand of the equation, represent the production and are exact. The pressure and the diffusion correlations need further modeling (the reader can find the details for these terms in to the work of Craft (1998)). Additionally, the dissipation rate ε_{ijk} is modeled using the isotropic dissipation. Fortunately, there is no need to solve one additional equation for the transport of the triple correlations. Craft (1998) suggested neglecting the convection terms in the left side of Eq. (4). Thus, he obtained a set of an algebraic system of equations, which is solved in a simple manner. The solution of the triple correlations is used to model the diffusion term. During our first runs, the adoption of Eq. (4) gave some problems primarily focused on the unstable behavior of the solver. Thus, we have decided to perform the computations with the generalized gradient diffusion hypothesis (GGDH) of Daly and Harlow (1970) which models the turbulent diffusion term using the equation:

$$d_{ij} = \frac{\partial}{\partial x_k}\left[\left(\nu\delta_{kl} + 0.22\overline{u_k u_l}\frac{k}{\varepsilon}\right)\frac{\partial \overline{u_i u_j}}{\partial x_l}\right] \tag{5}$$

In any case this ad hoc action generates some skepticism and undoubtedly further attempts should be made in order to obtain a fully-converged solution using the original formulation.

3. Numerical aspects and computational details

For the flow modeling, an in-house academic elliptic incompressible Navier–Stokes solver has been used. The solver uses the non-staggered arrangement in a structured grid for the solved flow parameters and a second-order scheme for the interpolation of the convective terms, Zhu (1991). The computational domain started at a distance equal to $4.5H$ upstream of the bend and extended to a distance up to $30H$ after the bend. During our first attempts to model the flow, both the non-linear and the Reynolds-stress models presented unstable behaviors. For this reason, some stability measures have been introduced to the solver. For the non-linear model, the proposed techniques by Craft et al. (1999) improved the stability, although it has been experienced that performing some preliminary iterations using the linear model and then switching to the non-linear could provide a very stable behavior towards convergence. Regarding the Reynolds-stress model, various techniques have been tested in order to ensure stability. It was found that the most effective techniques were the clipping techniques for the A and A_2 parameters (for the definition of these parameters, see Craft, 1998), and also the clipping for the lower positive bounds of the normal Reynolds stresses, turbulent Reynolds number and turbulence dissipation rate. Additionally, the special treatment for the positive and negative source terms in the discretized Reynolds-stress transfer equations has been found to be very helpful. Details for the latter technique can be found in the paper of Craft et al. (1999). Finally, a relatively small under-relaxation factor for these variables, usually equal to 0.1, contributed in a positive manner to a stable convergence. Table 1 summarizes the adopted stability measures and their level of success.

It is well understood that the correct inlet conditions contribute a lot to the quality of the predictions and also, to the fair assessment of an adopted model. For the inlet conditions, the interpolated and adapted to the grid points, inlet experimental values, have been used and special care has been taken in order to have the exact inlet conditions for all the flow parameters. Similar values with the ones used at the inlet section have been used for the total flow field, including a transformation also for the curved area of the duct, in order to setup the initial values. For the LEVM, a turbulent length scale equal to $0.5H$ has been used. This value gave in the core regions of the flow, Reynolds-stress distributions which are identical with the measured ones.

The solver has been parallelized for execution on a small computer cluster of 8 dual CPUs. For the parallelization, the MPI protocol has been adopted. The flow domain was divided to 16 sub-domains, each of them cor-

Table 1
Summary of the stability measures and their level of success

	NLEVM	RSM
Preliminary iterations using the LEVM	Good level of success	N/A The solver started with initial values for the Reynolds stresses based on the inlet values
Treatment of the source terms (based on their sign) in the turbulence energy and dissipation rate discretized equations	Good level of success	Applicable only for the turbulence dissipation rate discretized equation. Good level of success
Use of pseudoviscosities	Not used	Unsuccessful
Treatment of the source terms (based on their sign) in the discretized Reynolds-stress equations (only for the normal stress components)	Not applicable	Good level of success
Clipping of turbulence dissipation rate	Not used	Good level of success
Clipping of the negative values of the normal stress during an iteration	Not applicable	Good level of success
Clipping of the A and A_2 parameters during an iteration ($0 < A < 1$, $0 < A_2 < 8/3$)	Not applicable	Good level of success
Clipping of the turbulent Reynolds number $R_t = \max(0, R_t)$	Not used	Good level of success
Use of low values for the under-relaxation factors (the Reynolds-stress discretized equations)	Not used	Good level of success, very slow convergence

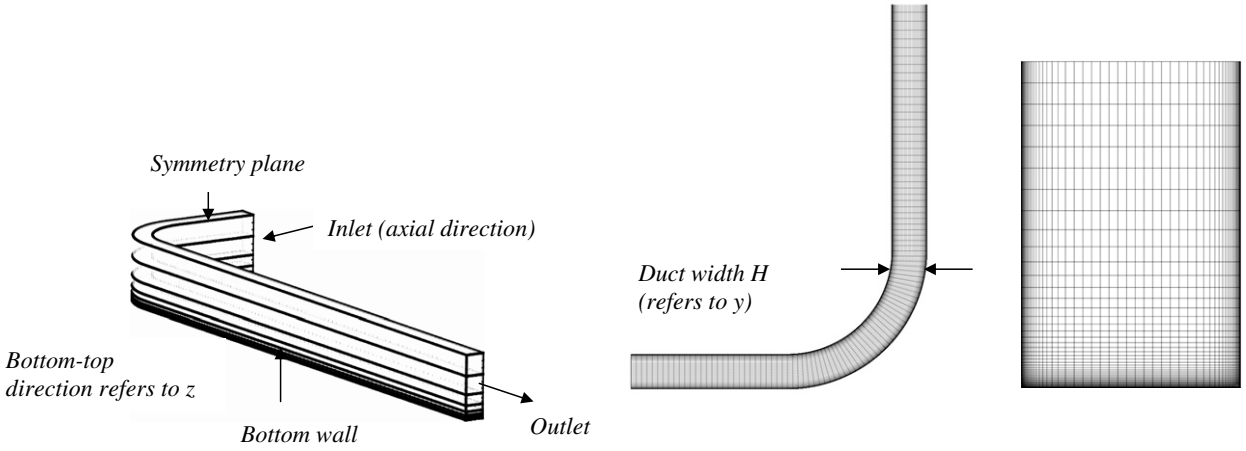

Fig. 1. Topology of the grid, sub-domains for parallel execution and two cross-sections showing the base grid.

responding to one CPU and special care has been taken in order to have a balanced problem to prevent any CPU from having "dead times" of waiting. Fig. 1 shows the topology of the duct with the sub-domains corresponding to each of the CPUs and two views of the grid. As the grid clustering is finer (towards the bottom wall), the splitting of the grid is performed to sub-domains having smaller size in the z-distance but the same number of grid points.

The convergence criterion has been chosen to be 1·E−05 for the dimensionless residuals (the dimensionalization was based on the inlet fluxes of the resolved flow quantities) of the main flow parameters. For the Reynolds-stresses, convergence occurred when the dimensionless residuals were four orders lower than the ones computed during the first iteration.

The grid dimensions (for the corresponding i,j,k indices) were $172 \times 138 \times 132$. These dimensions refer to the "base" grid. The typical user time for convergence was: 2 h for the LEVM, $2\frac{1}{2}$ h for the NLEVM and about 72 h for the RSM. Undoubtedly, the RSM is a big time-consumer but this can be related also to the small values of the under-relaxation factors used in order to have a stable convergence. For the grid-dependency studies, two additional grids were constructed having dimensions $172 \times 93 \times 84$ and $172 \times 48 \times 52$ (the alternative grid dimensions were chosen to be different only in the j and k planes where the duct walls are topologically placed). Regarding the y^+ values close to the wall it was ensured that at least for the two finer grids, 10 points in the normal to the wall direction had $y^+ < 0.1$ (the coarser grid gave corresponding values larger than 0.5 but not greater than 1). Undoubtedly, this value is very small, compared to a typical value, which is close to unity, but it was found that a fine grid resolution, close to the wall was needed in order to compute the complex derivatives appearing in the Reynolds-stress model without sudden divergence during the iterative computational procedure. Due to the limitations on memory and CPU resources, a grid having the double dimensions (for the three indices) was not tested. Thus, the grid-independency study is not a "proper" study although some indicative conclusions can be derived regarding the behavior of the models when similar grids with different sizes are used.

4. Results and discussion

4.1. Skin-friction coefficient and grid-dependency

The grid-dependency studies have been performed using the non-linear and the Reynolds-stress model and they were based on the skin-friction coefficient and velocity distributions. Figs. 2 and 3 show the comparative plots of the skin-friction coefficient computed by the non-linear eddy-viscosity model and the Reynolds-stress model, respectively, when the three grids are used. Especially for the RSM, it was impossible to obtain a successful convergence with the coarse grid. For the non-linear model, all the three grids present similar results. In the curved region of the duct, for the convex and concave walls, the base and the fine grid give nearly identical predictions. However, small differences occur in the distribution on the bottom wall but in general, the base and the fine grid provide results with close agreement. The same conclusions are derived for the Reynolds-stress model, Fig. 3. Both grids provide similar results. An intercomparison between the predictions obtained using the NLEVM and the RSM shows clearly that the first model gives better results for the skin-friction coefficient especially in the curved region of the duct. The RSM fails to capture the local distortion of the coefficient and tends to present a smoother distribution. Some explanations for this could be the use of the GGD hypothesis instead of the original proposed model for the triple correlations by Craft (1998).

Finally, in order to support the conclusions about the behavior of the models using different grids, the comparative plots of the velocity distributions obtained by the RSM, in the 45° station (as indicated in Fig. 1) and for $z/H = 0.5$, are presented, Fig. 4.

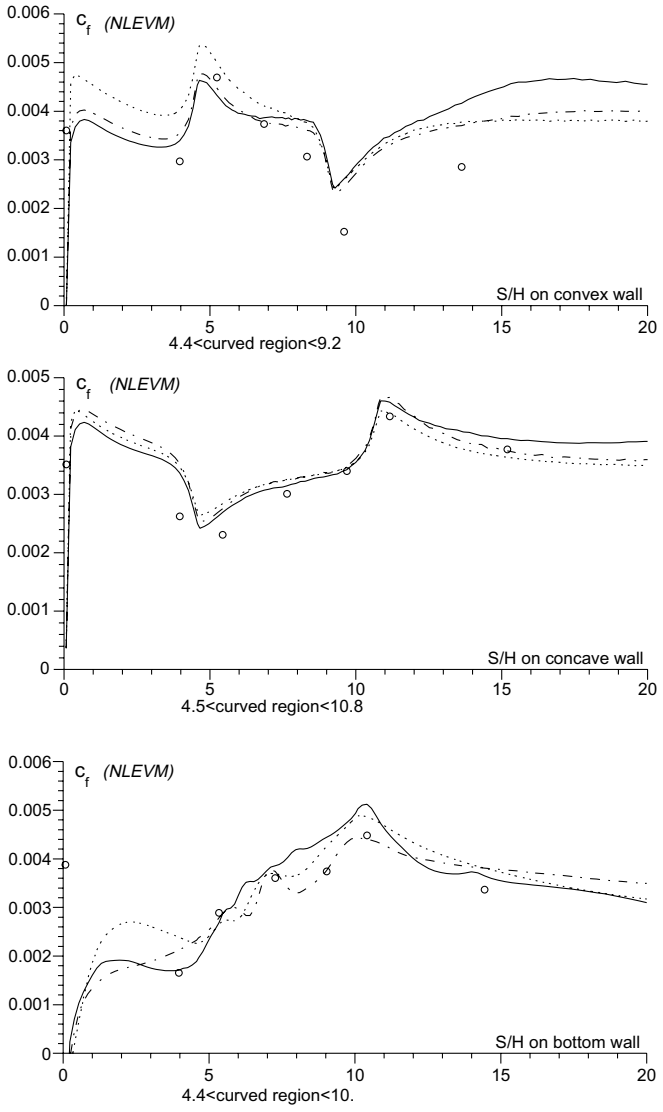

Fig. 2. NLEVM grid-dependency: skin-friction coefficient for the convex, concave and bottom wall. Circles: experimental values, solid line: finer grid, dot-dash line: base grid, dotted line: coarse grid.

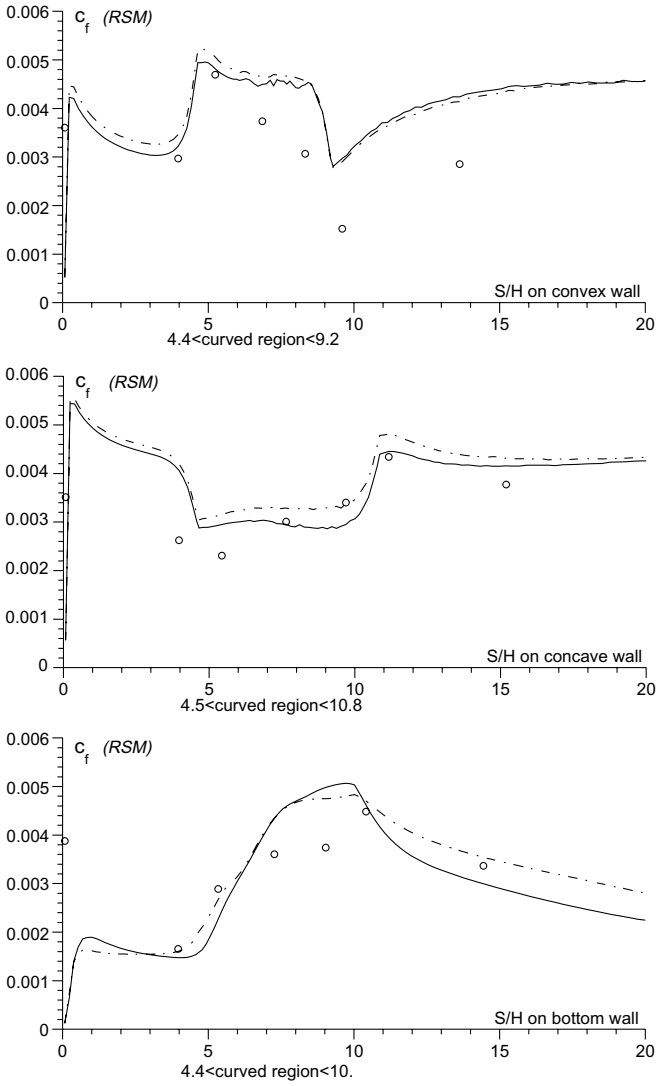

Fig. 3. RSM grid-dependency: skin-friction coefficient for the convex, concave and bottom wall. Circles: experimental values, solid line: finer grid, dot-dash line: base grid.

In general, the results obtained for skin-friction coefficient and the velocity distributions, are similar, although it cannot be concluded that the base grid is the one that can provide a grid-independent solution. It is clear that an additional investigation should be performed by having the full double grid in the three dimensions (and by continuing the study) but, as already written above, this was impossible due to the computer resource limits.

4.2. Predictions and detailed comparisons with the experimental measurements

The physics of the flow has been widely discussed by other researchers in the past. The basic mechanism of the flow development is strongly related to the duct's curvature, which generates a pressure field with different distribution from the convex to the concave wall. The longitudinal pressure distribution on the convex wall causes the flow to accelerate and this is clearly shown in the vector plots of the velocity distribution on the symmetry plane, for all the three models and in comparison with the measurements, Fig. 5a. As a general observation, the three models are able to predict the local acceleration of the axial velocity close to the convex wall. In a more detailed investigation, the maximum values of the axial velocity differ from model to model and this will be shown later. In Fig. 5b, the vector and contour plots of the velocity magnitude on the cross-section referring to the last station located at a distance 4.5H after the bend (coded as D2), are shown. In these plots, the left boundary is the convex wall, the right boundary is the concave wall and the upper and lower boundaries correspond to the top and bottom walls of the duct. The full three-dimensional regime of the flow starts to develop at the early stations of the bend. The flow forms two symmetrical vortices, which are devel-

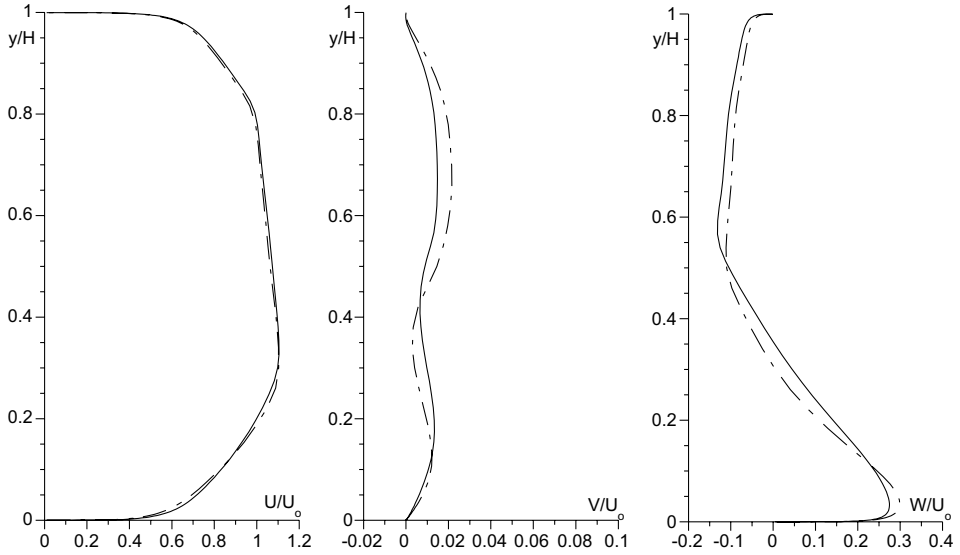

Fig. 4. RSM grid-dependency: velocity distributions at 45° station and for $z/H = 0.5$. Solid line: finer grid, dot-dash line: base grid.

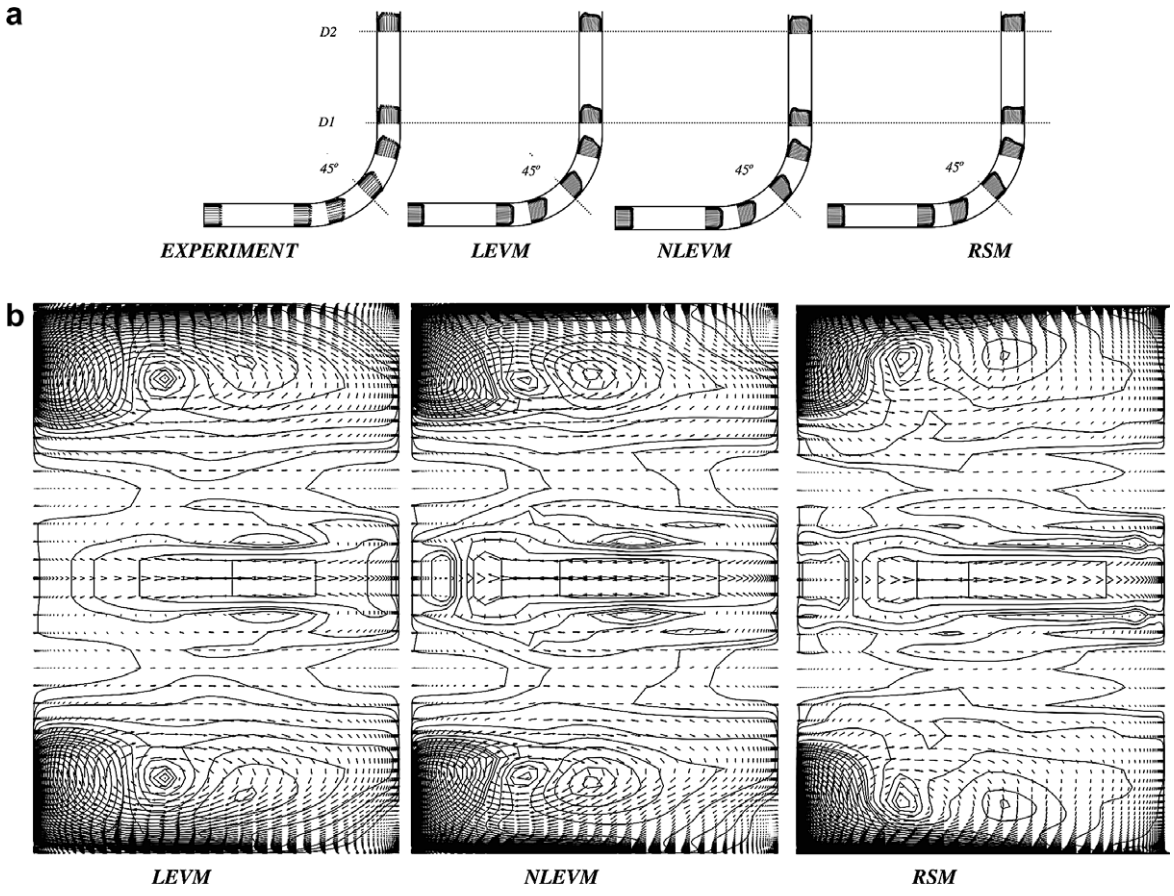

Fig. 5. Vector plots in the symmetry plane of the duct (a) and contour plots in the D2 cross-section (b).

oping until the exit of the duct. For each station, the size of the vortex located either to the top or bottom wall differs depending on the adopted model. At the 45° station (not shown here) the LEVM, predicts the vortex-center to be at a smaller distance from the convex wall than the two other models. At the D2 station (Fig. 5b) the behavior of the models changes. The LEVM and the NLEVM predict the location of the vortex-center closer to the symmetry plane. Finally, it has been found that the three models for all the cross planes, predict different vortex sizes.

The comparative plots of the computed and measured velocity and Reynolds-stress distributions for the measurement stations 45° and D1 give the appropriate information regarding the capability of the turbulence models to provide accurate predictions. In these plots, the velocity components have been nondimenionalized using the mean inlet velocity U_0 while the Reynolds-stresses have been nondimensionalized using the square of the mean inlet velocity (U_0^2). The distances have been nondimensionalized using the duct width H. For the same figures, $y/H = 0$ corresponds to the convex wall and $y/H = 1$ to the concave wall. Additionally, $z/H = 0.0625$ refers to the first measurement plane near the bottom wall of the duct, and $z/H = 3$ to the symmetry plane. As a general observation, both the Reynolds-stress and the non-linear models provided good predictions.

Since the experimental measurements have been carried out on a system following the spatial evolution of the duct-geometry, for the presentation of the computational results a transformation has been performed for the solved Cartesian velocity vector and the computed or solved Reynolds-stress tensor. The transformation matrix is given by $A = [a_{ij}]$, where a_{ij} refers to functions including the directional cosines. Thus, a vector is transformed using $\vec{V}_{\text{transformed}} = A \cdot \vec{V}_{\text{cartesian}}$ and a tensor is transformed using $T_{\text{transformed}} = A \cdot T_{\text{cartesian}} \cdot A^{\text{T}}$. From hereafter all the velocity components and the elements of the Reynolds-stress tensor will refer to their transformed values.

4.3. Measurement station 45°

Figs. 6 and 7 show the computed mean velocity profiles with the three adopted models and their comparison with the experimental data. Regarding the axial velocity component, U, the three models can provide quite satisfactory results. They can predict the general trend of the experimental distributions, which indicate a maximum value near the convex wall, shown also in the meridional cross-section of the duct in Fig. 5a. This maximum value is generated by the longitudinal negative pressure gradient along the convex wall, which by consequence accelerates the flow in the convex wall region. Among the three models, both the RSM and the NLEVM can predict this maximum value, although there are some small differences between them. The NLEVM predicts a thicker boundary layer on the convex wall. For the position located closer to the bottom wall ($z/H = 0.0625$, Fig. 6), the NLEVM computes correctly the boundary layer thickness and this holds also for the station located on the symmetry plane ($z/H = 3$, Fig. 7). On the other hand, the RSM computes a thinner boundary layer on the convex wall for the two z/H stations and it cannot capture exactly the axial-velocity maximum value (caused by the vortex pair) of the experimental data. Other stations (not shown here) showed similar trends. The linear model fails to provide good predictions in the convex wall region and systematically predicts a thicker boundary layer. In the core flow region ($0.2 < y/H < 0.7$) the RSM predictions for the axial velocity, are in good agreement with the experimental measurements. This observation is not valid for the first station at $z/H = 0.0625$, close to the bottom wall, where the model fails to predict a local distortion of the velocity located at $y/H = 0.5$. This local distortion is well predicted by the NLEVM although it has been found that the model underpredicts the axial velocity in the core region for stations located at $z/H = 0.5$ and $z/H = 0.75$ (both stations not shown here). For the symmetry plane, $z/H = 3$, the NLEVM predicts with a good accuracy the core flow region. The linear model for the z/H locations predicts larger axial velocity values than the measured ones.

As we move to higher y/H values, and in the concave wall region, the RSM predicts systematically a thinner

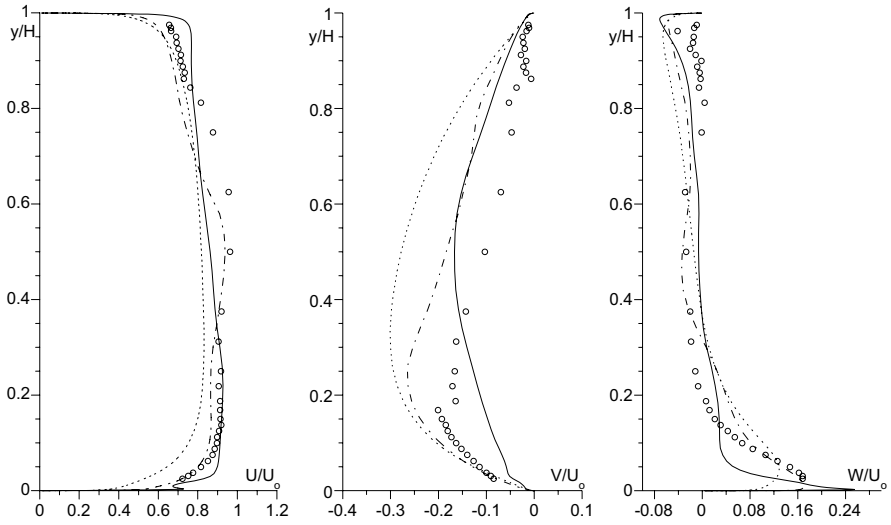

Fig. 6. Dimensionless velocity distribution at 45° measurement station and for $z/H = 0.0625$. Circles: experiment, dotted line: LEVM, dot-dash line: NLEVM, solid line: RSM.

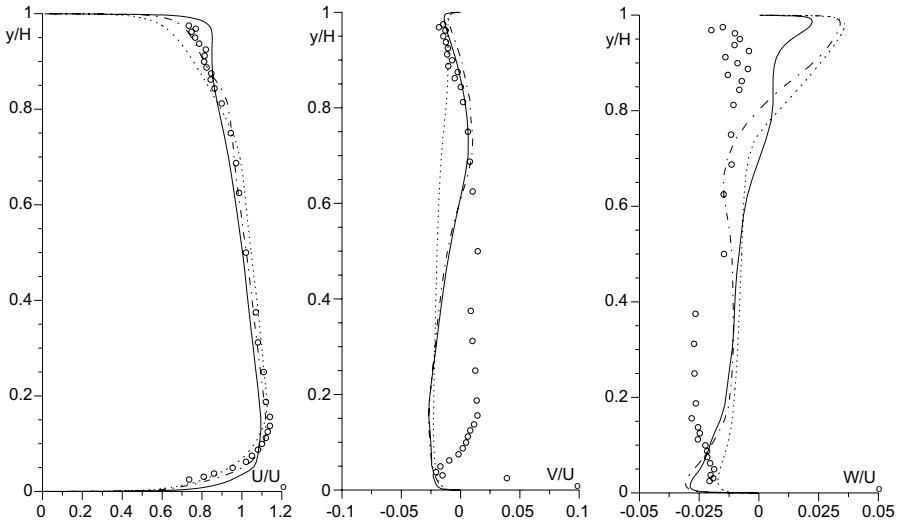

Fig. 7. Dimensionless velocity distribution at 45° measurement station and for $z/H = 3$ (symbols as in Fig. 6).

boundary layer, while the predictions of the NLEVM are closer to the measurements presenting thicker boundary layers, an observation noticed by Sotiropoulos and Ventikos (1998) also, when the k–ω cubic non-linear variant was adopted. The linear model also predicts thicker concave wall boundary layers.

The V- and W-velocity distributions, Figs. 6 and 7, show clearly the existence of the vortex pair formed in the convex wall region. Here, the RSM has a lower level of accuracy compared to the NLEVM. The latter proves capable in capturing well the V-velocity distribution in the convex wall region, at least for the first $z/H = 0.0625$ location. In the core region, and for the same velocity component, the NLEVM provides the best results. It can capture the trends of the velocity distributions, although it is not able to compute identical values to the measured ones. Systematically, it underpredicts the V-velocity values. On the other hand, the linear model and the Reynolds-stress model give results of lower quality. Finally, regarding again the V velocity, in the concave wall region all the models provide results of similar quality, which are very close to the experimental data. The same trends follow the predictions of the three models for the other stations, which are not shown.

The W-velocity component is generally well predicted by all the models, especially in the core region of the flow. The advantage of the RSM is clearly indicated in the region of the convex wall where the boundary layer thickness is computed to have the same thickness with the measured one. Again, the linear and the non-linear model predict thicker boundary layers. The quality of the predictions for all the models is lower in the concave wall region. Nevertheless, they provide acceptable results. All the models predict similar velocity distributions, except in the last z/H location where again the eddy-viscosity models compute larger and thicker boundary layers.

Figs. 8–10 show the results for the Reynolds-stress distributions. In the convex wall and core flow region, the model is able to provide acceptable distributions for the two stations and for all the stresses components. Apart from these two z/H stations, for the other stations (not shown here), similar behavior regarding the Reynolds-stress predictions from the RSM has been observed. On the other hand, the two eddy-viscosity models predict larger mean velocity fluctuations, especially inside the boundary layers developed on the convex wall. Additionally, the eddy-viscosity models systematically predict larger values for the Reynolds stresses in the core flow at the first location near the bottom wall ($z/H = 0.0625$, Fig. 8). In the concave wall region, the Reynolds-stress model fails to provide reasonable predictions. For this region, the experimental values show that the three normal Reynolds-stress components have relatively large values covering in some cases nearly the quarter of the duct width. The RSM presents the same trends with the experiments but it cannot capture the maximum values ($\overline{u'u'}$and $\overline{v'v'}$-components, Fig. 8). Additionally, the (lower) maximum values predicted by the model, are shifted towards the core flow in areas where the experiment shows that the flow has low turbulence. Again for the concave wall region, the two eddy-viscosity models seem to be able to represent correctly the normal Reynolds-stresses. For the symmetry plane ($z/H = 3$, Fig. 9) both the eddy-viscosity models provide far better results than the Reynolds-stress model. It has been found that this behavior is the same for the other z/H stations (not shown here), except the first one located in the bottom wall region. Finally, for the shear stresses, Fig. 10, again, the RSM provides very good results in the convex wall region but it cannot reproduce correctly the distributions in the concave wall region. The linear and non-linear model can provide results with better accuracy.

The station of 45° is characterized by the existence of the vortex pair generated from the two curved walls. The convex wall destabilizes the flow and this affects the predictions, especially the ones of the eddy-viscosity models.

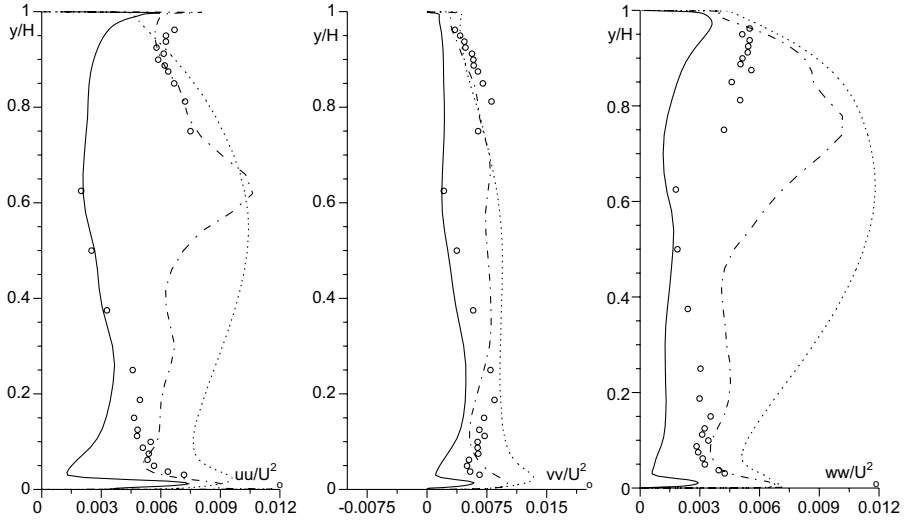

Fig. 8. Dimensionless normal Reynolds-stresses distribution at 45° measurement station and for $z/H = 0.0625$ (symbols as in Fig. 6).

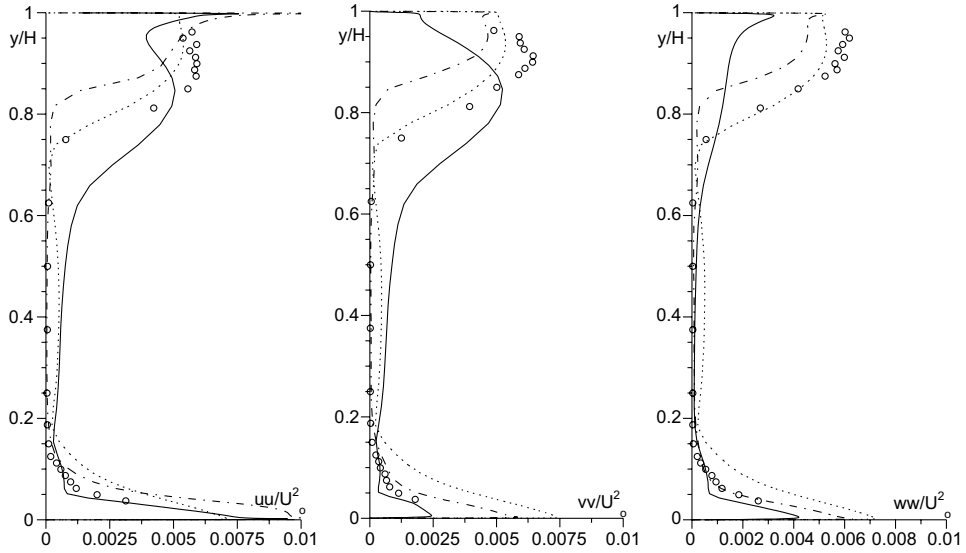

Fig. 9. Dimensionless normal Reynolds-stresses distribution at 45° measurement station and for $z/H = 3$ (symbols as in Fig. 6).

Both models, in the convex wall region, predicted thicker boundary layers in contrast to the Reynolds-stress model, which is able to overcome this problem. This specific capability of the RSM was shown also for the Reynolds-stress distributions in the convex wall region. The deficit of the Reynolds-stress model is related to its weakness to provide accurate results for the concave wall region. As the core flow comes from the straight part of the duct, it enters into the curved region by forming a small region where the flow stagnates before turning in order to follow the concave wall curvature. Probably, a better representation of the pressure term Π_{ij}, could resolve this problem. Of course, the use of the transport equation for the triple correlation as proposed by Craft (1998) should be tested but as already written, this was impossible in the present study.

4.4. Measurement station D1

Right after the bend, in the D1 cross-section, the flow is still fully three-dimensional. The two symmetrical vortices are developing in the cross-section up to the symmetry line between the bottom and the top wall. As Sotiropoulos and Ventikos (1998) refer, the measured values for the U-velocity component show an S-shaped distribution close to the convex wall, shown in Fig. 11. This axial velocity distortion is caused by the intense secondary motion. As we move to the symmetry plane, this motion spreads and the axial velocity profiles become again smooth and undistorted. The axial velocity distributions on the symmetry showed that the three models present similar results. As a first observation, in the convex wall region, again the two

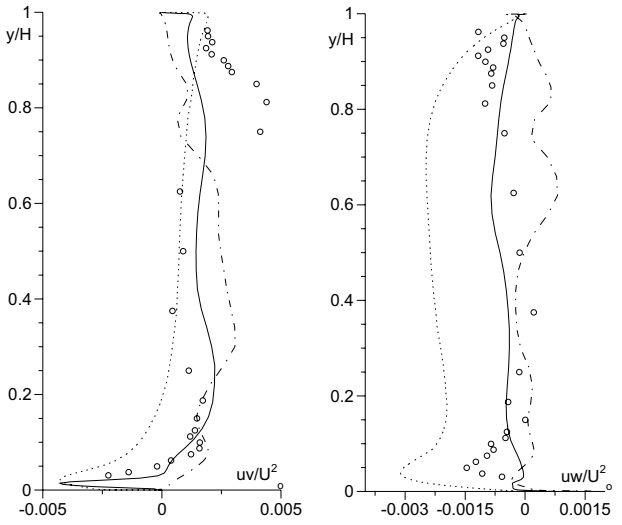

Fig. 10. Dimensionless shear Reynolds-stresses distribution at 45° measurement station and for $z/H = 0.0625$ (symbols as in Fig. 6).

eddy-viscosity models keep their tendency to overpredict the boundary layer thickness, while the RSM computes thinner boundary layers. One interesting point is that the non-linear model is able to capture the S-shaped distortion appearing at $z/H = 0.75$, Fig. 11, although it is clear that this region covers a larger distance in the y/H axis. The RSM is not able to predict such a distribution. Although it is difficult to conclude, it seems that the present results with the original variant of the Craft–Launder–Suga non-linear model show a better distribution of the axial velocity inside the S-shaped region than these of Sotiropoulos and Ventikos (1998) who used the same model but in the k–ω variant.

For the core flow region, all the models provide satisfactory results. A close investigation shows that the RSM is closer to the experimental measurements than the two eddy-viscosity models. Finally, in the concave wall region and again for the axial velocity, the RSM behaves as in the previous station, i.e., it calculates a thinner boundary layer. The linear and non-linear models, both predict thicker boundary layers, leading to the higher velocity values in the core flow region.

The existence of the intense secondary motion is also shown in the distributions of the V- and W-velocity components, Fig. 11. In the convex wall region, the V-velocity distributions are satisfactorily predicted by the RSM model but it is remarkable that the non-linear model can predict correctly the occurring local distortions between $y/H = 0.1$ and 0.4, although the maximum and the minimum experimental values cannot be captured. In the concave wall region, all the models provide similar results for the V-velocity.

Regarding the predictions of the W-velocity component, Fig. 11, the three models present similar results for $z/H = 0.75$. Small differences occurred in the convex wall region for the first plane close to the bottom wall, $z/H = 0.0625$ (not shown here), where the RSM predicts thinner boundary layer in contrast to the two eddy-viscosity models which present again, thicker boundary layers.

The Reynolds-stress distributions in the D1 measurement stations showed in general that the RSM gives better predictions in the convex wall region and this is true especially for the shear stresses. As in the 45° station, the RSM systematically underpredicts all the components of the Reynolds stresses, in the concave wall region. The Reynolds-stress model seems to overdump the turbulence in the concave wall and this could be possibly related to the computed distributions in the upstream flow region.

The observations regarding the behavior of the three models in the 45° and D1 stations are similar for the D2 station also. Due to the lack of space, additional figures will be not provided. For the axial velocity component, the three models provide similar results. In the convex wall region, the non-linear model gave the best predictions for

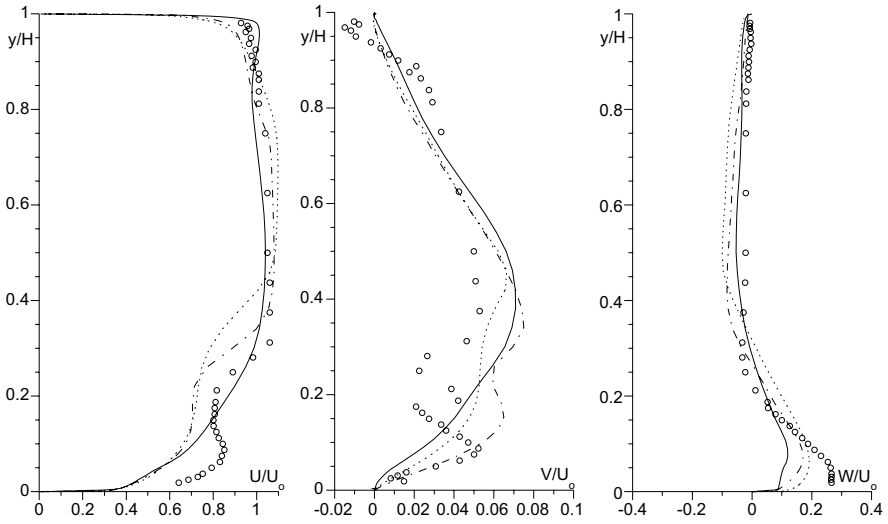

Fig. 11. Dimensionless velocity distributions at D1 measurement station and for $z/H = 0.75$ (symbols as in Fig. 6).

the boundary layer thickness. In the concave wall, the RSM predicted in an excellent manner the *U*-velocity distribution inside the boundary layer. The three models have predicted the *V*- and *W*-velocity components with a satisfactory quality. In some locations the differences were very small.

The results presented in this work have in general the same quality with the predictions obtained in previous works related to closed ducts. Although it is difficult to derive some strict conclusions when one has to compare all these sets together (because of the different quality and kind of the plots, etc.), in all the works it is clear that the curvature effects, especially the ones related to the flow destabilization, lead to the need of enhanced modeling. The main difference (and even additional point) between the already published works and the present work is that a very close investigation has been performed by trying to report all the steps during the modeling of the flow and by presenting comparisons not only for the velocity distributions but for all the Reynolds-stress components. This might be helpful for the final judgment regarding the quality of the predictions between three models.

5. Conclusions

The right choice of a turbulence model when an industrial turbulent flow problem is faced is a critical point, especially when this problem involves three-dimensional flow phenomena, which need an accurate modeling. Based on the application of three models, it has been shown in this study that the cubic non-linear eddy-viscosity model of Craft et al. (1996) can be a good first choice. It has the potential to provide rapid solutions with a quite satisfactory accuracy in conditions where curvature governs the flow development. This model is also able to give (with a lower quality) acceptable predictions for the Reynolds-stress distributions. The behavior of the model showed very clearly that it has been well calibrated although it seems that it needs further development in order to be able to capture the shear stress distributions near the wall regions where longitudinal pressure gradients occur. On the other hand, the Reynolds-stress model of Craft (1998) performed well for the majority of the velocity distributions. It must be noticed that generally it performed better in the representation of the Reynolds-stresses, especially the shear ones. Unfortunately we cannot conclude that it was found to be the best among the models since it could not provide good prediction for the concave wall region. One possible reason could be the adoption of the GGD hypothesis instead of the original proposition of Craft (1998). This could not be examined in the present work due to the major problems encountered when we tried to proceed with the original model. Finally, the linear model performed well in the predictions of the velocity distributions and surprisingly enough, in some predictions regarding the normal and shear stresses for the concave wall region where the longitudinal pressure distribution is not so strong as it is on the convex wall. Nevertheless, this study showed that this model can be an acceptable choice for a first indicative reproduction of this complicated flow field.

Of course, the main question remains: *is it worth proceeding with a complex turbulence model?* The answer should be given by considering many parameters, thus the choice it is left to the reader.

References

Abid, R., Rumsey, C., Gatski, T., 1995. Prediction of nonequilibrium turbulent flows with explicit algebraic stress models. AIAA J. 33, 2026–2031.

Cheah, S.C., Iacovides, H., Jackson, D.C., Ji., H., Launder, B.E., 1994. LDA investigation of the flow development through rotating U-ducts. In: Proc. Int. Gas-Turbine Congress and Exposition, ASME paper 94-GT-226.

Craft, T.J., 1998. Developments in a low-Reynolds-number second-moment closure and its application to separating and reattaching flows. Int. J. Heat Fluid Flow 19.

Craft, T.J., Launder, B.E., 1996. A Reynolds stress closure designed for complex geometries. Int. J. Heat Fluid Flow 17.

Craft, T.J., Launder, B.E., Suga, K., 1996. Development and application of a cubic eddy-viscosity model of turbulence. Int. J. Heat Fluid Flow 17.

Craft, T.J., Launder, B.E., Suga, K., 1997. Prediction of turbulent transitional phenomena with nonlinear eddy-viscosity model. Int. J. Heat Fluid Flow 18.

Craft, T.J., Iacovides, H., Yoon, J.H., 1999. Progress in the use of non-linear two-equation models in the computation of convective heat-transfer in impinging and separated flows. Flow Turbul. Combust. 63.

Daly, B.J., Harlow, F.H., 1970. Transport equations of turbulence. Phys. Fluids 13.

Davis, D.O., Gessner, F.B., 1992. Experimental investigation of turbulent flow through a circular-to-rectangular transition duct. AIAA J. 30, 367–375.

Ellis, L.B., Joubert, P.N., 1974. Turbulent shear flow in a curved duct. J. Fluid Mech. 62, 65–84.

Gatski, T.B., Speziale, C.G., 1993. On explicit algebraic stress models for complex turbulent flows. J. Fluid Mech. 254, 59–78.

Hanjalic, K., Launder, B.E., 1972. A Reynolds stress model of turbulence and its application to thin shear flows. J. Fluid Mech. 52.

Iacovides, H., Launder, B.E., Li, H.-Y., 1996a. Application of a reflection-free DSM to turbulent flow and heat transfer in a square-sectioned U-bend. Exp. Therm. Fluid Sci. 13, 419–429.

Iacovides, H., Launder, B.E., Li, H-Y., 1996b. The computation of flow development through stationary and rotating U-ducts of strong curvature. Int. J. Heat Fluid Flow 17, 22–33.

Kim, W.J., Patel, V.C., 1993. An experimental study of boundary-layer flow in a curved rectangular duct. In: Symposium on Data for Validation of CFD codes, ASME Fluids Eng. Div. Meeting, Washington, DC, FED-Vol. 16, pp. 13–28.

Launder, B.E., Sharma, B.I., 1974. Application of the energy-dissipation model of turbulence to the calculation of flow near a spinning disc. Lett. Heat Mass Transfer 1, 131–138.

Monson, D.J., Seegmiller, H.L., McConnayghey, P.K., Chen, Y.S., 1990. Comparison of experiment with calculations using curvature-corrected zero and two equation turbulence models for a two-dimensional U-duct, AIAA Paper 90-1484.

Palikaras, A., Yakinthos, K., Goulas, A., 2002. Transition on a flat plate with a semi-circular leading edge under uniform and positive shear free-stream flow. Int. J. Heat Fluid Flow 23.

Palikaras, A., Yakinthos, K., Goulas, A., 2003. The effect of negative shear on the transitional separated flow around a semi-circular leading edge. Int. J. Heat Fluid Flow 24.

Rumsey, C.L., Gatski, T.B., Morrison, J.H., 2000. Turbulence model predictions of strongly curved flow in a U-duct. AIAA J. 38, 1394–1402.

Smits, A.J., Young, S.T.B., Bradshaw, P., 1979. The effect of short regions of high surface curvature on turbulent boundary layers. J. Fluid Mech. 94, 209–242.

Sofialidis, D., Prinos, P., 1996. Wall suction effects on the structure of fully developed turbulent pipe flow. J. Fluids Eng. 188, 33–39.

Sotiropoulos, F., Ventikos, Y., 1998. Flow through a curved duct using nonlinear two-equation turbulence models. AIAA J. 36, 1256–1262.

Tamamidis, P., Assanis, D.N., 1993. Prediction of three-dimensional steady incompressible flows using body-fitted coordinates. ASME J. Fluids Eng. 115, 457–462.

Zhu, J., 1991. A low diffusive and oscillation free convection scheme. Commun. Appl. Numer. Methods 7.